

### Electronic Supplementary Information

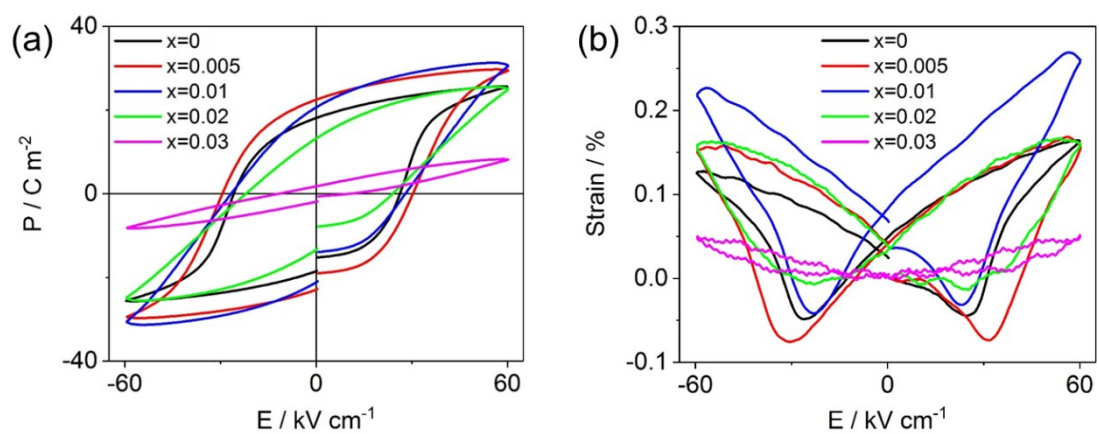


Figure S1 (a) Bipolar P-E loops; (b) Bipolar S-E loops for BF-BT-xNLN ceramics.

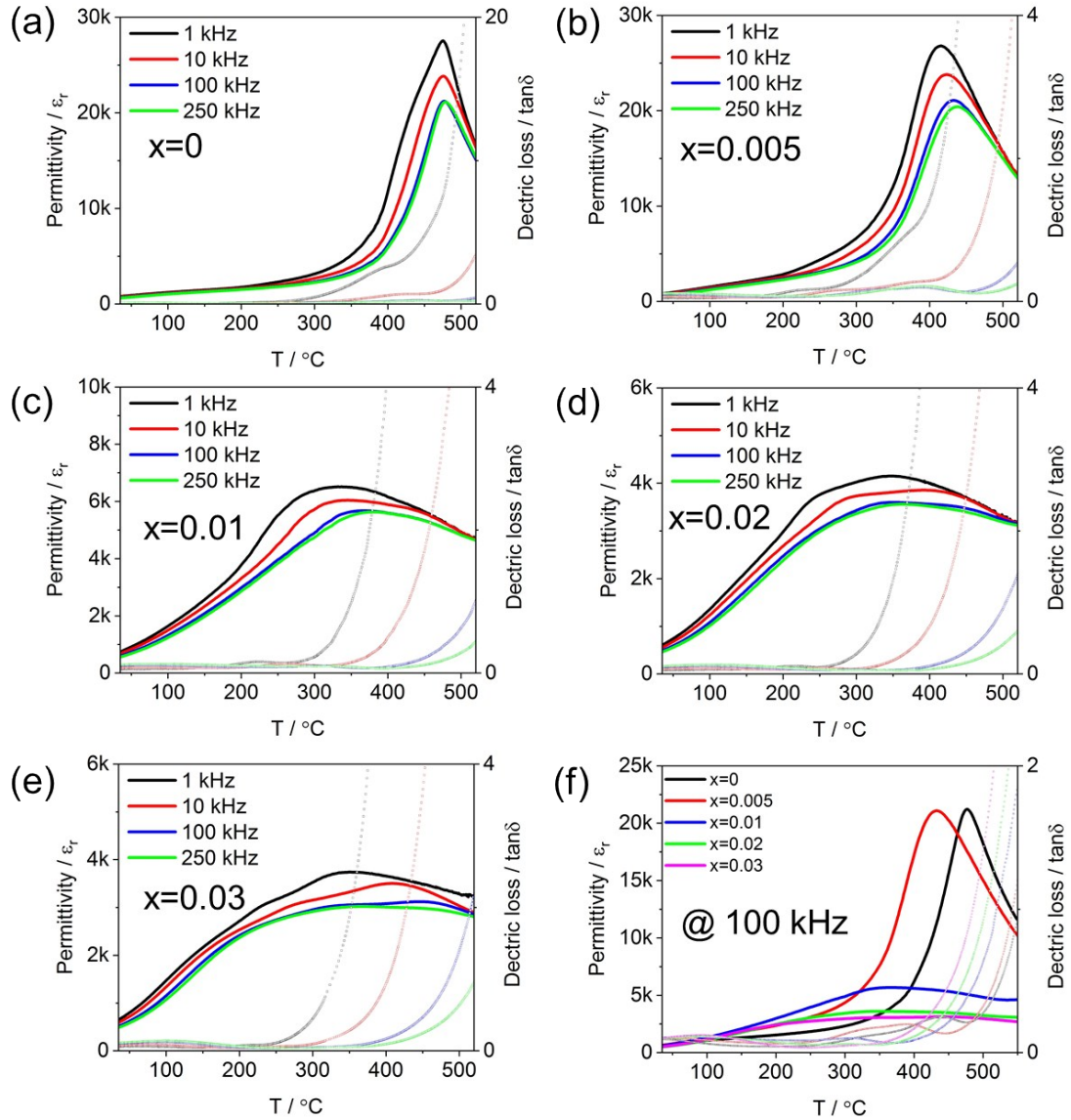


Figure S2. Frequency-dependent permittivity and loss curves for BF-0.3BT-xNLN with (a)  $x=0$ , (b)  $x=0.005$ , (c)  $x=0.01$ , (d)  $x=0.02$  and (e)  $x=0.03$ ; (f) Temperature-dependent permittivity and loss curves at 100 kHz for BF-BT-xNLN ceramics.

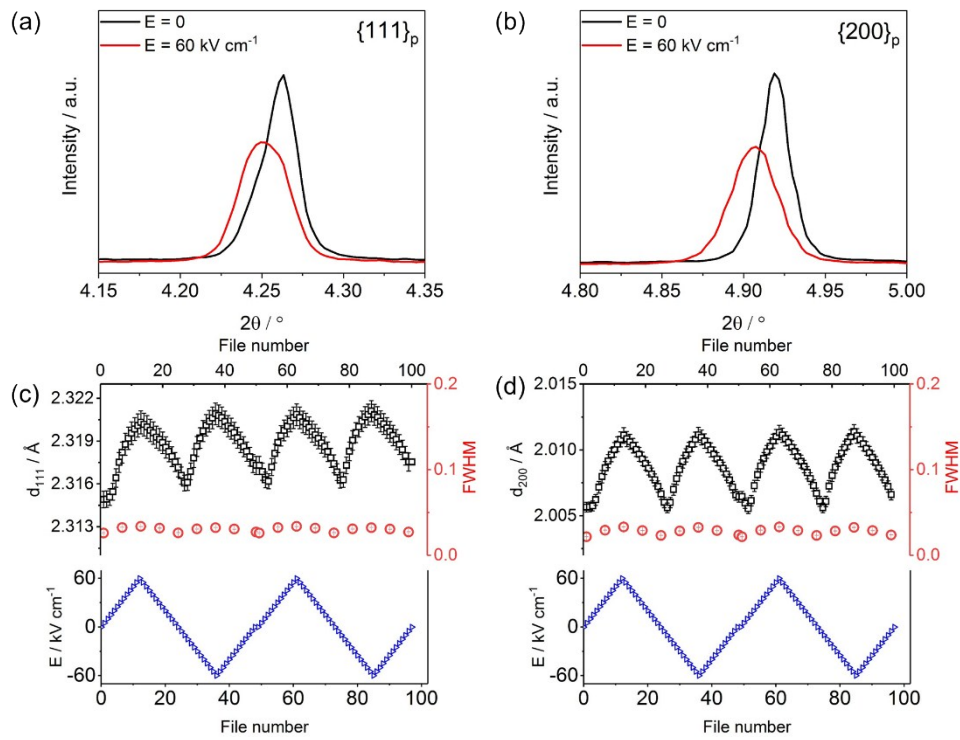


Figure S3. (a)  $\{111\}_p$  and (b)  $\{200\}_p$  XRD reflections at 0 and  $60 \text{ kV cm}^{-1}$  for BF-0.3BT at  $\beta = 0^\circ$ ; d-spacing and FWHM of (c)  $\{111\}_p$  and (d)  $\{200\}_p$  XRD reflection at  $\beta = 0^\circ$  obtained from the *in-situ* XRD experiment for BF-0.3BT, with two cycles of electric field poling under  $\pm 60 \text{ kV cm}^{-1}$

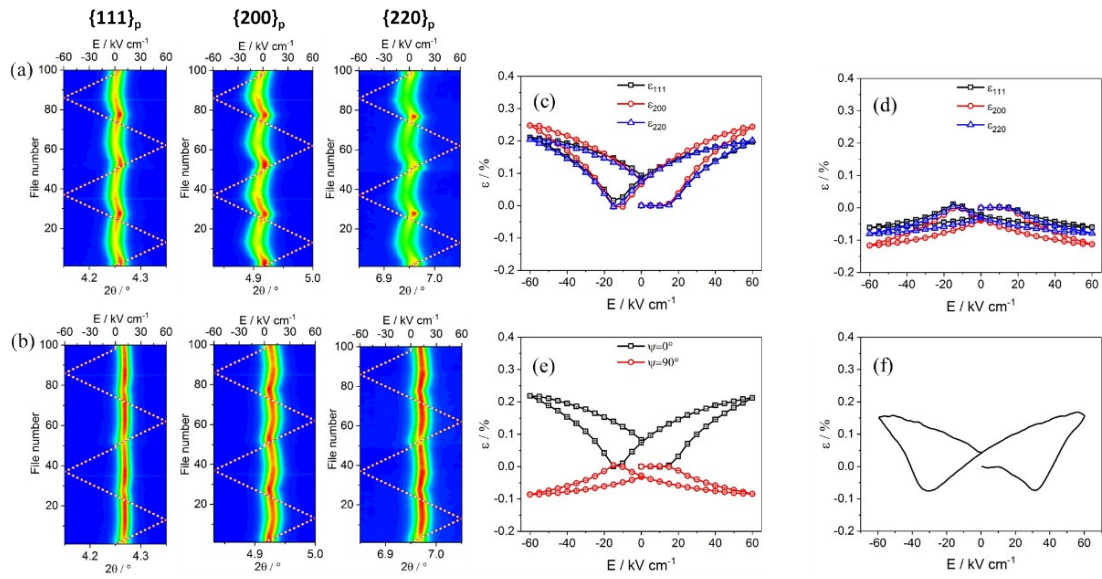


Figure S4. Contour plots of the  $\{111\}$ ,  $\{200\}$  and  $\{220\}$  peak profiles at (a)  $\beta = 0^\circ$  and (b)  $\beta = 90^\circ$  obtained from the *in-situ* XRD experiment for BF-0.3BT-0.005NLN, with two cycles of electric field poling under  $\pm 60 \text{ kV cm}^{-1}$ ; effective lattice strains calculated from representative peaks with grain orientations of (c)  $\beta = 0^\circ$  and (d)  $\beta = 90^\circ$  for BF-0.3BT-0.005NLN; (e) Total estimated macroscopic strain for  $\beta = 0^\circ$  and  $\beta = 90^\circ$  for BF-0.3BT-0.005NLN; (f) Directly measured macroscopic S-E loop for BF-0.3BT-0.005NLN.

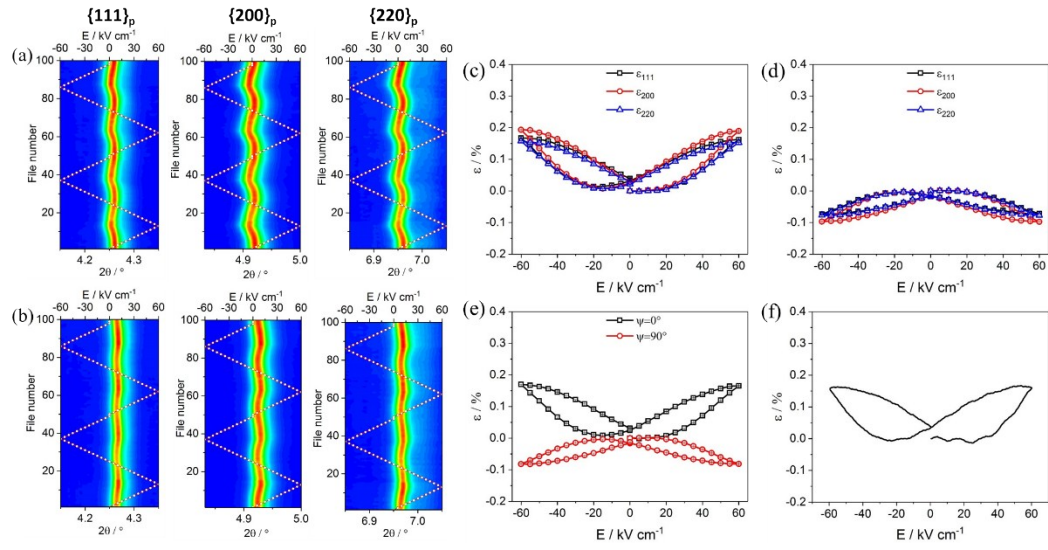


Figure S5 Contour plots of the  $\{111\}_p$ ,  $\{200\}_p$  and  $\{220\}_p$  peak profiles at (a)  $\beta = 0^\circ$  and (b)  $\beta = 90^\circ$  obtained from the *in-situ* XRD experiment for BF-0.3BT-0.02NLN, with two cycles of electric field poling under  $\pm 60 \text{ kV cm}^{-1}$ ; Effective lattice strains calculated from representative peaks with grain orientations of (c)  $\beta = 0^\circ$  and (d)  $\beta = 90^\circ$  for BF-0.3BT-0.02NLN; (e) Total estimated macroscopic strain for  $\beta = 0^\circ$  and  $\beta = 90^\circ$  for BF-0.3BT-0.02NLN; (f) Directly measured macroscopic S-E loop for BF-0.3BT-0.02NLN.

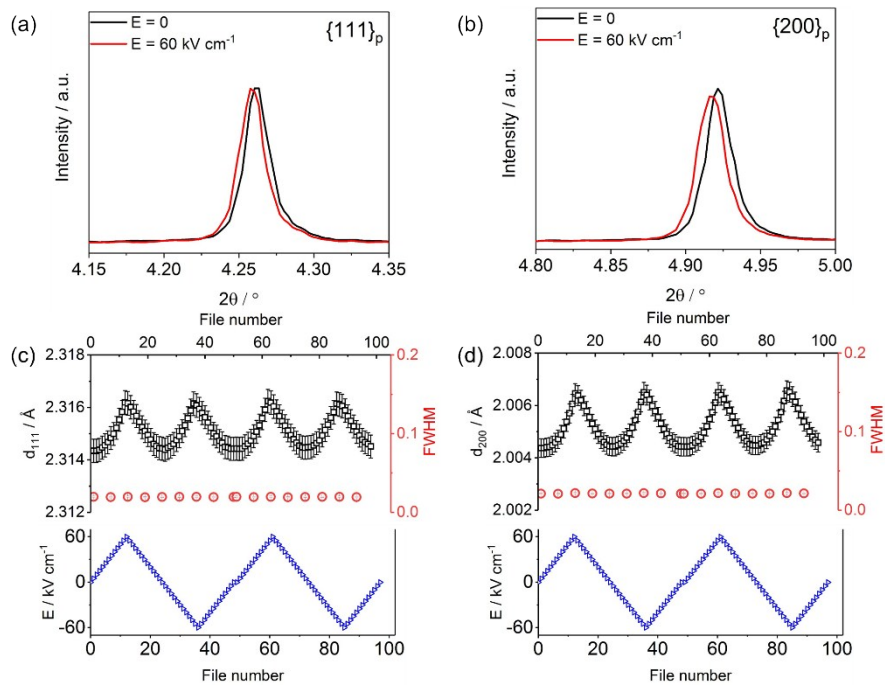


Figure S6. (a)  $\{111\}_p$  and (b)  $\{200\}_p$  XRD reflections at 0 and  $60 \text{ kV cm}^{-1}$  for BF-0.3BT-0.03NLN at  $\beta = 0^\circ$ ; d-spacing and FWHM of (c)  $\{111\}_p$  and (d)  $\{200\}_p$  XRD reflection at  $\beta = 0^\circ$  obtained from the *in-situ* XRD experiment for BF-0.3BT-0.03NLN, with two cycles of electric field poling under  $\pm 60 \text{ kV cm}^{-1}$ .

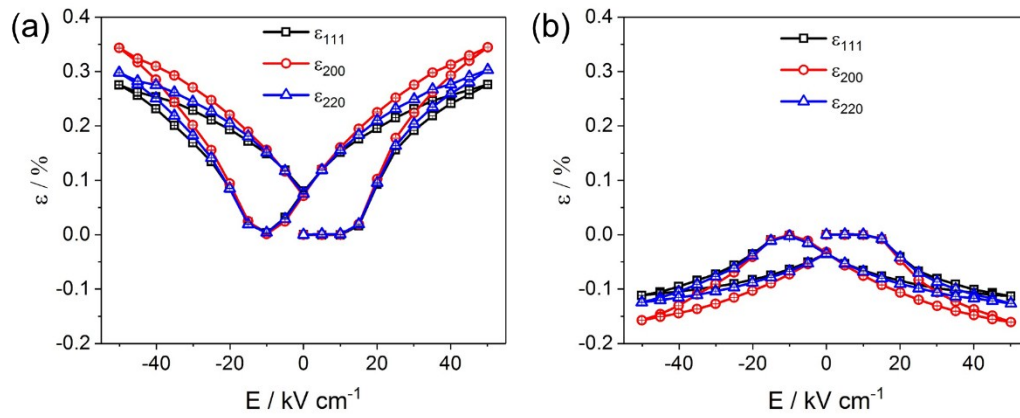


Figure S7 Effective lattice strains calculated from representative peaks with grain orientations of (a)  $\beta = 0^\circ$  and (b)  $\beta = 90^\circ$ , obtained from the *in-situ* XRD experiment for 5%BiScO<sub>3</sub> doped BF-BT ceramics, with two cycles of electric field poling under  $\pm 50$  kV cm<sup>-1</sup>

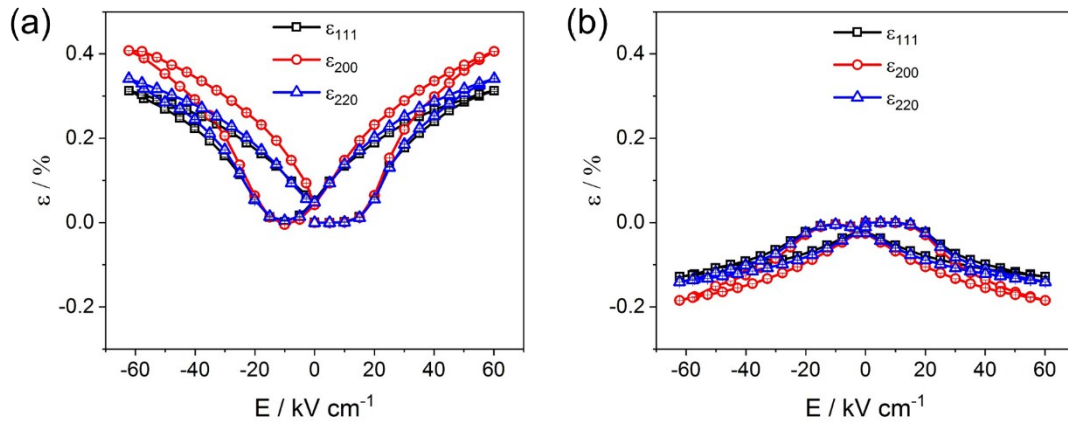


Figure S8 Effective lattice strains calculated from representative peaks with grain orientations of (a)  $\beta = 0^\circ$  and (b)  $\beta = 90^\circ$ , obtained from the *in-situ* XRD experiment for 5%BiMg<sub>2/3</sub>Nb<sub>1/3</sub>O<sub>3</sub> doped BF-BT ceramics, with two cycles of electric field poling under  $\pm 60 \text{ kV cm}^{-1}$